Published in final edited form as:
J Chem Neuroanat. 2009 October ; 38(2): 106–116. doi:10.1016/j.jchemneu.2009.05.002.

Regional and laminar distribution of the vesicular glutamate transporter, VGluT2, in the macaque monkey auditory cortex

Troy A. Hackett and **Lisa A. de la Mothe**
Vanderbilt University School of Medicine, Department of Hearing and Speech Sciences

Abstract

The auditory cortex of primates contains thirteen areas distributed among three hierarchically-connected regions: core, belt, and parabelt. Thalamocortical inputs arise in parallel from four divisions of the medial geniculate complex (MGC), which have regionally-distinct projection patterns. These inputs terminate in layers IIIb and/or IV, and are assumed to be glutamatergic, although this has not been verified. In the present study, immunoreactivity (-ir) for the vesicular glutamate transporter, VGluT2, was used to estimate the regional and laminar distribution of the glutamatergic thalamocortical projection in the macaque auditory cortex. Coronal sections containing auditory cortex were processed for VGluT2 and other markers concentrated in the thalamorecipient layers: cytochrome oxidase, acetylcholinesterase, and parvalbumin. Marker expression was studied with wide field and confocal microscopy. The main findings were: 1) VGluT2-ir was highest in the core, intermediate in the belt, and sparse in the parabelt; 2) VGluT2-ir was concentrated in the neuropil of layers IIIb/IV band in the core and layer IIIb in the belt and parabelt; 3) VGluT2-ir matched regional and laminar expression of the other chemoarchitectonic markers. The results indicate that the glutamatergic thalamic projection to auditory cortex, as indexed by VGluT2-ir, varies along the core-belt-parabelt axis in a manner that matches the gradients of other markers. These chemoarchitectonic features are likely to subserve regional differences in neuronal activity between regions of auditory cortex.

INTRODUCTION

The auditory cortex of primates contains 13 areas distributed among three regions: core, belt, and parabelt (Hackett, 2007a; Kaas et al., 2000) (Fig. 1a). The regions are interconnected in a manner consistent with a three-tiered processing hierarchy, where information appears to flow from the core to the belt, then on to the parabelt (Fig. 1b). In addition to cortical connection patterns, the division of auditory cortex into regions is supported by additional anatomical features.

First, each region of primate auditory cortex receives a different blend of inputs from the four major divisions of the medial geniculate complex (MGC) (de la Mothe et al., 2006b; Hackett et al., 1998b; Hackett et al., 2007; Jones, 2007; Molinari et al., 1995; Morel et al., 1992; Morel et al., 1993) (Fig. 1b). The main inputs to the core region arise from the tonotopically organized ventral division (MGv), which is an extension of the primary subcortical pathway. The belt region mainly receives inputs from the posterodorsal (MGpd) and anterodorsal (MGad)

Correspondence to: Troy A. Hackett, Vanderbilt University, Department of Hearing and Speech Sciences, 301 Wilson Hall, 111 21st Avenue South, Nashville, TN 37203, Phone: 615.322.7491, Email: troy.a.hackett@vanderbilt.edu.

subdivisions of the dorsal division (MGd). The parabelt region receives mainly MGpd inputs, fewer inputs from the MGad no clear inputs from the MGv. All three regions receive inputs from the magnocellular, or medial, division (MGm).

Second, the chemoarchitecture of auditory cortex varies by region. The most robust feature is that the neuropil of the main thalamorecipient layers (IIIb and IV) stains darkly for several markers: acetylcholinesterase (AChE), cytochrome oxidase (CO) and parvalbumin (PV) (de la Mothe et al., 2006a; Hackett et al., 1998a; Hackett et al., 2001; Jones, 2003; Jones et al., 1995; Morel et al., 1992; Morel et al., 1993). Marker expression in the layer IIIb/IV band is greatest in the core, intermediate in the belt, and weakest in the parabelt region. This density gradient reflects progressive reductions in both staining density and width of the IIIb/IV band along the core-belt-parabelt axis. Although the functional significance of these anatomical gradients is not well-understood, it is reasonable to suppose that they contribute to activity-related differences between regions.

Considered together, thalamocortical input patterns and chemoarchitectonic marker distribution tend to covary along the core-belt-parabelt axis. Systematic decreases in layer IIIb/IV marker density are accompanied by shifts in the origin and laminar distribution of thalamic and cortical inputs, suggesting that these anatomical gradients are functionally linked. On the assumption that such gradients reflect activity-related differences between regions, we were led to consider whether there may also be gradients in the distribution of glutamatergic inputs along the core-belt-parabelt axis. Glutamate is widely assumed to be the principal excitatory neurotransmitter in cortex, and is well-established as the primary excitatory neurotransmitter released by thalamocortical afferents in the auditory cortex (Cruikshank et al., 2002; Kharazia et al., 1994; LeDoux et al., 1991; Popowits et al., 1988). Accordingly, glutamatergic thalamocortical terminals should be concentrated in the IIIb/IV band, and in a manner that reflects the sublaminar projection patterns of each MGC division.

As an index of this feature, widefield and confocal microscopy were combined to study immunohistochemical expression of the vesicular glutamate transporter, VGluT2, in the macaque monkey auditory cortex. Vesicular glutamate transporters (VGluTs) regulate glutamate storage and release in synaptic vesicles (Fremeau et al., 2004a; Fremeau et al., 2004b; Kaneko et al., 2002a; Kaneko et al., 2002b). The mRNA of the VGLuT1 and VGLuT2 isoforms are widely expressed by glutamatergic neurons in the spinal cord, brainstem, thalamus and cortex, although expression patterns vary between structures (Fremeau et al., 2004a; Fremeau et al., 2001; Hur et al., 2005; Nahmani et al., 2005). In some areas, VGluT1 and VGluT2 have been found in synapses with low and high release probability, suggesting that the two transporters reflect distinct classes of glutamatergic projections with complementary distribution patterns and functional roles (Kaneko et al., 2002a; Varoqui et al., 2002). In sensory systems, however, their segregation is not complete. In the primary somatosensory cortex (S1) of mice, Graziano et al (2008) reported that the laminar distributions of VGLuT1 and VGluT2 immunoreactive terminals were partly overlapping. Specifically, VGluT2 immunoreactive (-ir) terminals were concentrated in layer IV, whereas VGluT1-ir terminals were concentrated in layers I–III, and less dense in layer IV. This pattern is comparable to other studies in which VGLuT2-ir was concentrated in layer IV terminals of visual and somatosensory cortex (Fujiyama et al., 2004; Kaneko et al., 2002b). Graziano et al (2008) also found that both transporters were colocalized in many layer IV terminals. This appears to confirm an earlier observation in rats in which VGluT1 and VGluT2 mRNA were co-expressed in nearly all neurons in the primary sensory relay nuclei of the thalamus (Barroso-Chinea et al., 2007). In the MGC, VGluT1 mRNA expression was confined to the MGv, whereas neurons expressing VGluT2 were widely distributed in all divisions. In consideration of all of these findings, then, it appears that VGluT2-ir is a general marker of the glutamatergic thalamocortical projection to auditory cortex, whereas VGluT1-ir is associated both with corticocortical projections

involving the supragranular layers, and the MGv projection to layer IV of A1 and perhaps other core areas.

MATERIALS AND METHODS

Tissue acquisition and histology

All procedures involving animals were conducted in accordance with international standards on animal welfare, followed NIH Guidelines for the Care and Use of Laboratory Animals, and were approved in advance by the Vanderbilt University Institutional Animal Care and Use Committee. Temporal lobes were obtained postmortem from two macaque monkeys (*M. radiata*). The animals were deeply anesthetized by a lethal dose of pentobarbital. Immediately after cardiac arrest the animal was perfused through the heart with 1 liter each of the following solutions prepared in 0.1 M phosphate buffer (pH 7.4): 0.9% saline, cold (4° C) 4% paraformaldehyde, and cold (4° C) 4% paraformaldehyde plus 10% sucrose. Following perfusion the brains were removed and photographed. The cerebral hemispheres were separated from the thalamus and brainstem, blocked, and placed in 30% sucrose for 1 to 3 days. Blocks containing auditory cortex were cut frozen at 40 μm on a sliding microtome in an off-coronal plane, perpendicular to the long axis of the temporal lobe. Alternating series of sections were processed for Nissl (N) using thionin, acetylcholinesterase (AChE)(Geneser-Jensen et al., 1971), cytochrome oxidase (CO)(Wong-Riley, 1979), myelinated fibers (MF)(Gallyas, 1979), and immunohistochemistry for parvalbumin (PV), vesicular glutamate transporter 2 (VGluT2), and the neuron specific protein, NeuN (details below). Some series were reacted for VGluT2 and PV or VGluT2 and NeuN using dual fluorescence immunohistochemistry.

Immunohistochemistry

In each animal, two to three adjacent series of sections were reserved for immunohistochemical detection of VGluT2, PV, and NeuN with monoclonal antibodies and fluorescent secondary antibody conjugates. All antibodies used are commercially available and have been well characterized (Table 1). Sections reserved for sequential double or triple-fluorescent immunohistochemistry were rinsed in 0.01M phosphate buffered saline and 1% Triton X-100 (PBS-Tx) (pH 7.4), incubated for 2 hours at room temperature in blocking solution (3% normal goat serum in 0.01M PBS-Tx), then incubated for 48 hours at 4° C in blocking solution containing the primary antibody at the concentration listed in Table 1. After this incubation, sections were rinsed in PBS, then incubated for 24 hours at 4° C in a 1:200 solution of 0.01M PBS containing one of three Alexa-fluor secondary anti-IgG conjugates (Invitrogen) (Table 1). Thereafter, sections were rinsed in PBS, and incubated in the second or third primary/secondary antibody combination. For each run, control sections not incubated in the primary antibody were reserved for comparison with reacted sections. Those comparisons revealed no cross-reactivity between antibodies. After completion of all incubations, sections were mounted on glass slides, coverslipped, and stored at 4° C in the dark.

As an additional control, a separate series of sections was reacted for VGluT2 alone using the same primary antibody, but with a standard avidin-biotin complex reaction (Vector Labs PK 6200) in place of the fluorescent secondary. Briefly, prior to incubation in the primary antibody, endogenous biotin was blocked using an avidin-biotin blocking kit (Vector Labs SP 2001). Sections were rinsed in PBS and incubated in the primary antibody as described above. This was followed by incubations for 2 hours in the biotinylated secondary antibody (horse anti-mouse, 1:200), and 2 hours in the avidin-biotin complex. The substrate reaction was performed with the Vector Labs VIP kit (SK-4600).

Microscopy

Reacted tissue sections were examined under brightfield or fluorescent illumination on a Nikon E80i microscope, equipped with filter cubes matching the emission spectra of the fluorescent secondary antibodies (405, 488, 594 nm), and a dual FITC/TRITC cube for visualizing red and green fluorescence simultaneously. Digital images were acquired with an MBF CX9000 camera and Neurolucida 7.0 software (Microbrightfield, Inc.). Image montages were acquired with the Virtual Slice plugin for Neurolucida. Images were cropped, and adjusted for brightness and contrast.

Confocal image stacks of double-and triple-labeled fluorescent material were obtained using an Olympus Fluoview 1000 laser scanning confocal microscope equipped with 405 nm diode laser, and Argon 488, and 543 lasers, 60x Plan Apochromatic objective (NA 1.42), pinhole size of 1 Airy unit (zoom = 2). Resolution was 103 nm/pixel in the X and Y dimensions (1024 × 1024 pixels/frame), and step size in the z-dimension was 0.74 um. Three-dimensional image stacks were obtained with the Olympus Fluoview viewer (V1.6a), then exported to ImageJ (NIH) for additional analysis.

RESULTS

Histochemical and Immunohistochemical Expression Patterns

Series of adjacent sections were processed to reveal PV-ir andVGluT2-ir (dual fluorescence), CO, AChE, MF, and Nissl in coronal sections of the macaque monkey auditory cortex in the caudal two-thirds of the temporal lobe. Illustrated in Figures 2 and 3 are low magnification images of adjacent sections stained for these markers at the level of A1 and R, respectively. Two major features are noted here. First, the expression PV-ir, VGluT2-ir, CO and AChE was concentrated in an overlapping horizontal band in the middle layers of cortex, corresponding to the layer IIIb/IV band. Second, expression density in the IIIb/IV band was highest in the core (A1, R), intermediate in the surrounding belt areas (MM, ML, RM, AL), and weakest in the parabelt (CPB, RPB), reflecting a descending gradient along the core-belt-parabelt axis. In the AChE preparation, additional bands of intense staining were located in layers I and Vb. Comparable patterns were observed in sections stained for myelinated fibers (MF). In the core, MF staining had an astriate pattern, typical of the core region, in which laminae III – VI are made indistinct by the dense matrix of horizontal and vertical (radial) fibers (see Hackett et al 2001). The belt and parabelt areas had a bistriate pattern of myelination, in which the bands of horizontal fibers in layers IV and Vb are visible due to reductions in the density of the intervening laminae. Overall, myelin density was lower in the parabelt. Contrasting with weak density in layer II, MF staining in layer I was prominent across all areas, as it was in the AChE preparation.

In Figures 4 and 5, the laminar distribution of these markers is shown at higher magnification. In the core, VGluT2-ir was concentrated in the neuropil of layers IIIb and IV (upper portion), overlapping dense PV-ir and staining for CO and AChE (demarcated by arrowheads). VGluT2-ir along the border between layers IV and Va was sharp and cleanly demarcated, whereas staining at the upper border of IIIb diminished more gradually. Similar patterns characterized the expression of PV, AChE and CO in the neuropil of the IIIb/IV band, indicating that the laminar distribution of these markers is highly overlapping. Also visible in the core at this level of magnification was a very weak band of VGluT2-ir in layer Vb/VI, overlapping the relatively prominent band of AChE staining in the same layer. In the belt areas, VGluT2-ir was concentrated in layer IIIb, with limited involvement of the upper half of layer IV. As in the core, PV-ir and histochemical staining of CO and AChE were coextensive with VGluT2-ir. VGluT2-ir IIIb of the parabelt was weaker than all other areas examined, matching that of the other markers.

In addition to its expression in the neuropil of the layer IIIb/IV band, PV-ir was located in the somata and dendrites of neurons in all areas of auditory cortex. Typically, the PV-ir neurons were scattered throughout layers II – VI. Although generally less numerous in layer IV, there was a slight tendency for PV-ir cells to be concentrated along the border of layer IV and V.

Double Fluorescent Labeling of NeuN + VGluT2

Sections processed for double fluorescent labeling of the neuron-specific antibody (NeuN) and VGluT2 were used to verify the laminar expression patterns of VGluT2 observed in adjacent sections stained for various markers (above), and to more carefully study their co-expression with the aid of the confocal microscope. Epifluorescent (Fig. 6) and high-magnification montages of confocal image stacks (Fig. 7) were obtained from adjacent areas of the core, belt and parabelt at the level of A1.

Confirming observations from inspection of adjacent sections stained for different markers, VGluT2 expression in A1 (green) was concentrated in the neuropil among the small (granule) NeuN-ir cells of layer IV (red) and extended into layer IIIb, which contained larger NeuN-ir pyramidal neurons (Figs. 6a, 7). The NeuN-ir cells in layer IV of A1 were arranged in well organized vertical columns that could be followed well into layer III and sometimes into layer II. VGluT2-ir was concentrated around cell columns, creating a strong columnar appearance in A1. In layer VI (Fig. 6e), a relatively sparse band of VGluT2-ir was formed by the local branching of axons. These were studded by immunoreactive densities, likely boutons *en passant*. From the confocal images (Fig. 7), it can be seen that VGluT2-ir was concentrated in the neuropil surrounding cell soma, presumably on dendrites (Graziano et al., 2008), which were not well-defined by the NeuN antibody. Somata were not immunoreactive for VGluT2.

In the belt areas (MM, ML), the VGluT2-ir band was narrower than A1, and concentrated in layer IIIb (Fig. 6b, c). In area MM, medial to A1, VGluT2-ir in this band was moderately dense, but reduced compared to A1 and extended slightly into layer IV. VGluT2-ir in the layer IIIb band of area ML was less dense compared to MM. The columnar distribution of labeling in belt was not as clear as in A1, especially for ML where labeling was the weakest. As in A1, VGluT2-ir was concentrated in the neuropil of MM and ML, with sparse labeling on somata (Fig. 7b, c). VGluT2-ir in the IIIb/IV band of the parabelt (Fig. 6d) was rarely detected. As in the core, a weak band of VGluT2-ir was found in layer VI of belt and parabelt areas (Fig. 6f–h), characterized by the local branching of axons studded by numerous boutons en passant.

DISCUSSION

The purpose of the present study was to reveal the regional and laminar distribution of VGluT2 in auditory cortex of the macaque monkey, and relate those findings to established patterns of thalamocortical and corticortical connections. The main findings of this study were: 1) VGluT2-ir in the macaque auditory cortex was concentrated in the neuropil of a horizontal band involving layers IIIb and IV, with weaker expression in layer VI; 2) VGluT2-ir in the IIIb/IV band was coextensive with the elevated expression of several markers, including PV, AChE, and CO; 3) the density of VGluT2-ir was highest in the core, intermediate in the belt, and sparse in the parabelt; 4) in the core region, VGluT2-ir was concentrated in layer IIIb and the upper half of IV; 5) in the belt and parabelt region, VGluT2-ir was focused in IIIb; 6) VGlutT2-ir densities were concentrated in the neuropil, presumably on dendrites. These findings are summarized in Fig. 8, and discussed in the sections that follow.

Regional differences in VGluT2 immunoreactivity

The division of auditory cortex into hierarchically organized regions is primarily based on anatomical gradients, such as neuronal architecture and connection patterns (Hackett, 2007a;

Kaas et al., 2000). The results of the present study add relevant new information about the distribution of glutamatergic inputs across regions. Most notably, we observed that VGluT2-ir in the thalamorecipient layers (IIIb, IV) varied systematically along the medial-lateral axis (i.e., between regions). Thus, the density of VGluT2-ir was highest in the core, intermediate in the medial and lateral belt, and very low in the parabelt (Fig. 8A). Moreover, VGluT2 density gradients closely matched those of PV, AChE, and CO established in the present and previous studies (de la Mothe et al., 2006a; Hackett et al., 1998a; Hackett et al., 2001; Jones et al., 1995). Their close correspondence implies that these markers are functionally related, and covary in a manner that reflects activity-dependent differences between regions.

For example, the concentration of CO in the layer IIIb/IV band of primary sensory areas is commonly thought to reflect elevated metabolic demands, as neuronal and synaptic densities are generally greater in these laminae (O'Kusky et al., 1982; Wong et al., 1998). PV expression is associated with neurons that can fire repeatedly at high rates (Rudy et al., 2001), and VGluT2 is often located in synapses with high-release probability (Fremeau et al., 2004a; Fremeau et al., 2004b; Varoqui et al., 2002). Accordingly, the elevated expression of CO, PV and VGluT2 in the thalamorecipient layers could be associated with higher activity levels, especially in the core region where the expression of these markers is greatest. Similarly, elevated AChE expression may reflect the dependence on acetylcholine release for synaptic and receptive field plasticity in layers III and IV which has been well documented in A1 (Rasmusson, 2000; Weinberger, 1995). The reduction of these markers in the belt and parabelt implies that neuronal activity changes systematically along the core-belt-parabelt axis. Although electrophysiological studies of the parabelt are currently lacking, studies of the core and belt areas have revealed differences in response properties of neurons along this axis, including increased tuning bandwidth and longer response latencies (Kajikawa et al., 2005; Lakatos et al., 2005; Rauschecker et al., 1995; Recanzone et al., 2000).

Laminar patterns of VGluT2-ir and relationship to thalamocortical inputs

The concentration of VGluT2-ir in the thalamorecipient layers of auditory cortex, especially the core region, matches laminar distribution patterns observed in studies of primary somatosensory and visual cortex (Fujiyama et al., 2004; Graziano et al., 2008; Kaneko et al., 2002b). Thus, elevated VGluT2-ir in the thalamorecipient laminae may be a common property of primary sensory cortex. Further, Graziano et al (2008) positively localized VGluT2 to axon terminals in layer IV of S1 cortex from neurons in the ventroposterior nucleus (VP) in the thalamus, suggesting that VGluT2-ir may be useful as a marker of glutamatergic thalamocortical projections. Given those findings, a number of anatomical observations from the present and previous studies can be tied together with important functional implications for auditory cortex.

As indexed by VGluT2-ir, the laminar patterns of glutamatergic thalamocortical projections to primate auditory cortex vary regionally. It is well established that the blend of inputs from each MGC division varies between regions of auditory cortex (de la Mothe et al., 2005; Hackett, 2007b; Hackett et al., 1998b; Hackett et al., 2007; Jones, 2007; Molinari et al., 1995; Morel et al., 1992; Morel et al., 1993). Generally, neurons in the MGv target the core region, neurons in the dorsal divisions (MGad, MGpd) target the belt and parabelt regions, and the MGm targets all areas (Fig. 8C). In addition, the average density of these projections appears to vary somewhat between regions (Fig. 8A, C). Following tritiated proline injections into divisions of the MGC and adjoining nuclei in monkeys, Jones and Burton (1976) found that the density of labeled terminals was highest in the core (A1) and moderate to high in areas corresponding to the belt and parabelt. Thus, in the core and belt regions, VGluT2-ir and thalamocortical terminal density is corresponding. In the parabelt region, however, where VGluT2-ir was very

sparse or absent, Jones and Burton (1976) found that terminal density was not significantly lower than in the belt areas.

These results suggest several possible, and perhaps related, explanations. First, VGluT2-ir in auditory cortex may largely reflect inputs from the primary (MGv) pathway (Fig. 8C). Although the MGv projection mainly targets areas in the core region, weaker MGv inputs to some areas in the belt region have been observed (Hackett et al., 2007;Molinari et al., 1995;Morel et al., 1992;Morel et al., 1993), but not to the parabelt (Hackett et al., 1998b). Thus, if VGluT2-ir is a selective marker of the glutamatergic MGv projection, the gradient in its projections could account for the systematic decreases in VGluT2-ir observed along the core-belt-parabelt axis. This explanation is probably incomplete, however, since neurons expressing VGluT2 mRNA are widely distributed throughout the MGC in rats (Barroso-Chinea et al., 2007). Thus, VGluT2-ir in the belt areas could reflect projections from a subpopulation of neurons in the MGad, MGpd, or MGm. This would not explain the absence of VGluT2 in the IIIb/IV band of the parabelt, however.

A second and closely related possibility is that VGluT2 is expressed by a subpopulation of neurons distributed in variable proportions among the divisions of the MGC (Fig. 8B, E). For example, each MGC division contains distinct neuronal subpopulations immunoreactive for the calcium-binding proteins parvalbumin (PV-ir) or calbindin (CB-ir) (Hashikawa et al., 1991; Hashikawa et al., 1995; Jones, 2003; Molinari et al., 1995). The PV-ir neurons project to layers IIIb and IV, whereas the CB-ir neurons mainly project to superficial layers (I – III). The MGv, which primarily targets the core region, is dominated by the PV-ir population. The MGad, which mainly projects to caudal belt areas, such as MM and CM (de la Mothe et al., 2006b; Hackett et al., 2007; Molinari et al., 1995), also has a dominant PV-ir population, but has more CB-ir neurons than the MGv. The MGpd and MGm have comparable numbers of both cell types. So, the relative numbers of PV-ir neurons in each MGC division is positively correlated with the relative differences in VGluT2 density observed between the core and belt regions in the present study. The PV-VGluT2 combination does not account for the near absence of VGluT2-ir in the parabelt, however, since the MGpd appears to contain equal numbers of PV-ir and CB-ir neurons and its projection to the parabelt is comparable in density to the belt (Jones and Burton, 1976). On the other hand, since it has not been established that PV-ir neurons in the MGpd project to the parabelt, this remains an open question.

A third explanation could be that glutamatergic neuronal subpopulations across the MGC utilize different and perhaps unknown glutamate transporters. Currently, three VGluT isoforms are known. VGluT3 does not appear to be widely distributed in cortex and is therefore not a likely alternative. As for VGluT1, Graziano et al (2008) found that the laminar patterns of VGluT1 and VGluT2 protein expression in S1 were largely complementary. VGluT1-ir was concentrated in layers I – III and reduced in layer IV, whereas VGluT2-ir was concentrated in layer IV, with a secondary band in layer VI. Similar patterns were evident in A1 and V1, as well. However, judging from the images provided, there was no evidence that VGluT1 was upregulated in secondary areas surrounding A1, S1 or V1. Thus, while VGluT1-ir and VGluT2-ir have complementary laminar patterns, regional patterns are overlapping in sensory cortex of the mouse. Since we did not study VGluT1 in the present study, the possibility that one or both are more heavily expressed by neurons that project to the belt and parabelt areas cannot be ruled out, but several pieces of evidence render this explanation highly doubtful. In the recent study of VGluT1 and VGluT2 expression in the thalamus of rats (Barroso-Chinea et al., 2007), VGluT2 mRNA was widely expressed by neurons in all MGC divisions, whereas VGluT1 mRNA expression was found only in the MGv, and at slightly reduced levels. Expression patterns were similar in VP and the lateral geniculate nucleus (LGN). Moreover, the mRNA of both transporters was co-expressed by most or all neurons in the principal relay nuclei, supporting the additional finding of Graziano et al (2008) that VGluT1-ir and VGluT2-

ir were frequently colocalized in the same axon terminals in layer IV of S1 of the mouse. Thus, the absence of VGluT1 mRNA from the MGd and the coexpression of both transporters in the MGv suggest that the regional distributions of VGluT1-ir and VGluT2-ir will be comparable and will diminish along the core-belt-parabelt axis.

A fourth explanation is that methodological factors or anatomical differences in the axonal projections of a subpopulation of MGC neurons restricts immunohistochemical detection of VGluT transporters. Since little is known about the ultrastructure of those neurons and their cortical terminations, this remains speculative.

Clearly, additional studies will be needed to address the questions that have been raised here. In the meantime, we can conclude that there is a strong correspondence between VGluT2-ir and at least a portion of the total thalamocortical projection to the core and belt regions.

Sublaminar patterns of VGluT2-ir

Thalamic input to auditory cortex from the MGC is typically reported to be concentrated in layers IIIb and IV, with weaker direct or collateral inputs to other laminae (de Venecia et al., 1998; Hashikawa et al., 1991; Hashikawa et al., 1995; Jones et al., 1976; McMullen et al., 1993; Velenovsky et al., 2003). It is often overlooked, however, that sublaminar input patterns are not uniform across areas. In primates, for example, MGv projections to the core are distributed over layers IIIb and IV, whereas inputs to the belt and parabelt from the MGpd and MGad are concentrated in IIIb, with limited or sparse projections into the upper portion of IV (Hashikawa et al., 1995; Jones et al., 1976; Mesulam et al., 1973). Similar findings have been reported in the cat (Shinonaga et al., 1994). These patterns closely match the sublaminar distribution of VGluT2-ir in the present study. In areas A1 and R of the core, VGluT2-ir was concentrated in layer IIIb and the upper half of layer IV, and reduced in the lower half of layer IV. In the belt areas, VGluT2-ir was concentrated in IIIb, with minimal extension into the upper edge of layer IV.

These observations highlight basic regional differences in the circuitry that require further study (Fig. 8F). The absence of thalamic input to layer IV of the belt and parabelt raises intriguing questions concerning the nature of those inputs. What is their source(s)? Are they glutamatergic? The predominant theory, which has a measure of anatomical support, is that layer IV of the belt and parabelt receives inputs from at least one other auditory area (de la Mothe et al., 2006a;Fitzpatrick et al., 1980;Galaburda et al., 1983). This raises the additional question (discussed above) concerning the identity of the glutamate transporter or neurotransmitter used in those projections, since VGluT2-ir was sparse or absent from layer IV, and VGluT1 and VGluT3 are doubtful candidates (Barroso-Chinea et al., 2007;Graziano et al., 2008). Assuming that glutamate is the principal excitatory neurotransmitter in these circuits, it may be that feedforward cortical projections to layer IV between areas of auditory cortex utilize a glutamate transporter that has not been identified, or perhaps VGluTs are not an adequate marker of certain types of glutamatergic projections. These questions will need to be addressed if we are to fully understand information flow and the interactions between parallel inputs to a given area of auditory cortex. This is discussed briefly below.

Implications for information processing in auditory cortex

Information processing in auditory cortex reflects the summation of activity mediated by a complex network of connections involving several nuclei in the thalamus (MGC, other) and dozens of auditory and auditory-related cortical areas. Unfortunately, our current understanding of information flow in these circuits is rudimentary. Although the principal input and output sources for most areas have been identified, the manner in which those connections are integrated (i.e., laminar, columnar, cellular interactions) are largely unknown. Thus, the

influence of a given input source on auditory processing within an area or region is rather difficult to predict.

Although many questions remain unanswered, the results of the present study represent an important step toward the characterization of these circuits, and may even have functional implications for the major circuits that have been identified. For example, a basic tenet of our working model of primate auditory cortex organization is that information processing is hierarchical along the core-belt-parabelt axis (Kaas et al., 1998; Kaas et al., 2000). This hypothesis is supported by the diminishing VGluT2-ir gradient along the same axis. In brief, the direct influence of this class of glutamatergic inputs within the processing hierarchy is limited to the thalamorecipient layers of the core and belt. The findings also imply that the influence of glutamatergic inputs regulated by VGluT2 represents a minor fraction of the total 'excitatory' inputs to a given area or even a single column of cells. We must add to this, of course, the influence of GABA-ergic, serotonergic, cholinergic, and noradrenergic inputs from sources that have not yet been integrated into our working model. Thus, the regional and laminar patterns of VGluT2-ir observed in the present study support the processing hierarchy, but also remind us that many details remain to be worked out.

CONCLUSIONS

The main finding of this study indicates that VGluT2-ir is concentrated in the thalamorecipient layers of the macaque monkey auditory cortex, but diminishes in magnitude along the core-belt-parabelt axis, matching chemoarchitectonic gradients of other markers concentrated in those layers. The regional and laminar distribution of VGluT2-ir closely matches the thalamocortical projection patterns of the MGv, which also diminishes along this axis, suggesting that VGluT2-ir may largely reflect the inputs of the primary (lemniscal) pathway. Since the density of thalamocortical axon terminals is only partially reduced along the core-belt-parabelt axis, glutamatergic projections not regulated by VGluT2 may utilize a different transporter. The results also revealed that VGluT2-ir was largely absent from layer IV in the belt and parabelt regions, a potential target of feedforward connections between auditory areas. The absence of VGluT2 from those projections suggest that these circuits utilize a different glutamate transporter, as well. Overall, the findings are consistent with the serial flow of information along the core-belt-parabelt axis, but highlight the need for detailed exploration of the chemical anatomy of these circuits.

Acknowledgments

The authors gratefully acknowledge the support of NIH/NIDCD grant RO1 DC04318 to T.A. Hackett and T32 MH075883 to Vanderbilt Kennedy Center for support of the confocal microscope.

List of Abbreviations

A1	uditory area 1 (core)
AChE	Acetylcholinesterase
AL	Anterolateral area (belt)
CB	Calbindin
CL	Caudolateral area (belt)
CM	Caudomedial area (belt)
CO	Cytochrome oxidase

CPB	Caudal parabelt area (parabelt)
CS	Central sulcus
Ins	Insula
IPS	Intraparietal sulcus
LGN	Lateral geniculate nucleus
LS	Lateral sulcus
LuS	Lunate sulcus
MGad	Medial geniculate complex, anterodorsal division
MGC	Medial geniculate complex
MGd	Medial geniculate complex, dorsal division
MGm	Medial geniculate complex, magnocellular division
MGpd	Medial geniculate complex, posterodorsal division
MGv	Medial geniculate complex, ventral division
ML	Middle lateral area (belt)
MM	Middle medial area (belt)
Pro	Proisocortical area
proA	Prokoniocortex area
PS	Principal sulcus
PV	Parvalbumin
R	Rostral area (core)
Ri	Retroinsular area
RM	Rostromedial area (belt)
RPB	Rostral parabelt area (parabelt)
RT	Rostrotemporal area (core)
RTL	Rostrotemporal lateral area (belt)
RTM	Rostrotemporal medial area (belt)
STG	Supeior temporal gyrus
Tpt	Temporal parietotemporal area
VGluT	Vesicular glutamate transporter
VP	Ventroposterior nucleus

References

Barroso-Chinea P, Castle M, Aymerich MS, Perez-Manso M, Erro E, Tunon T, Lanciego JL. Expression of the mRNAs encoding for the vesicular glutamate transporters 1 and 2 in the rat thalamus. J Comp Neurol 2007;501:703–15. [PubMed: 17299752]

Cruikshank SJ, Rose HJ, Metherate R. Auditory thalamocortical synaptic transmission in vitro. J Neurophysiol 2002;87:361–84. [PubMed: 11784756]

de la Mothe LA, Blumell S, Kajikawa Y, Hackett TA. Thalamocortical connections of core and medial belt auditory cortex in marmoset monkeys. Assoc Res Otolaryngol Abs 2005:67.

de la Mothe LA, Blumell S, Kajikawa Y, Hackett TA. Cortical connections of auditory cortex in marmoset monkeys: core and medial belt regions. J Comp Neurol 2006a;496:27–71. [PubMed: 16528722]

de la Mothe LA, Blumell S, Kajikawa Y, Hackett TA. Thalamic connections of auditory cortex in marmoset monkeys: core and medial belt regions. J Comp Neurol 2006b;496:72–96. [PubMed: 16528728]

de Venecia RK, Smelser CB, McMullen NT. Parvalbumin is expressed in a reciprocal circuit linking the medial geniculate body and auditory neocortex in the rabbit. J Comp Neurol 1998;400:349–62. [PubMed: 9779940]

Fitzpatrick KA, Imig TJ. Auditory cortico-cortical connections in the owl monkey. J Comp Neurol 1980;192:589–610. [PubMed: 7419746]

Fremeau RT Jr, Voglmaier S, Seal RP, Edwards RH. VGLUTs define subsets of excitatory neurons and suggest novel roles for glutamate. Trends Neurosci 2004a;27:98–103. [PubMed: 15102489]

Fremeau RT Jr, Kam K, Qureshi T, Johnson J, Copenhagen DR, Storm-Mathisen J, Chaudhry FA, Nicoll RA, Edwards RH. Vesicular glutamate transporters 1 and 2 target to functionally distinct synaptic release sites. Science 2004b;304:1815–9. [PubMed: 15118123]

Fremeau RT Jr, Troyer MD, Pahner I, Nygaard GO, Tran CH, Reimer RJ, Bellocchio EE, Fortin D, Storm-Mathisen J, Edwards RH. The expression of vesicular glutamate transporters defines two classes of excitatory synapse. Neuron 2001;31:247–60. [PubMed: 11502256]

Fujiyama F, Kuramoto E, Okamoto K, Hioki H, Furuta T, Zhou L, Nomura S, Kaneko T. Presynaptic localization of an AMPA-type glutamate receptor in corticostriatal and thalamostriatal axon terminals. Eur J Neurosci 2004;20:3322–30. [PubMed: 15610164]

Galaburda AM, Pandya DN. The intrinsic architectonic and connectional organization of the superior temporal region of the rhesus monkey. J Comp Neurol 1983;221:169–84. [PubMed: 6655080]

Gallyas F. Silver staining of myelin by means of physical development. Neurol Res 1979;1:203–9. [PubMed: 95356]

Geneser-Jensen FA, Blackstad TW. Distribution of acetyl cholinesterase in the hippocampal region of the guinea pig. I. Entorhinal area, parasubiculum, and presubiculum. Z Zellforsch Mikrosk Anat 1971;114:460–81. [PubMed: 5550728]

Graziano A, Liu XB, Murray KD, Jones EG. Vesicular glutamate transporters define two sets of glutamatergic afferents to the somatosensory thalamus and two thalamocortical projections in the mouse. J Comp Neurol 2008;507:1258–76. [PubMed: 18181146]

Hackett, TA. Organization and correspondence of the auditory cortex of humans and nonhuman primates. In: Kaas, J., editor. Evolution of the Nervous System. Elsevier; Oxford: 2007a. p. 109-119.

Hackett, TA. Organization of the thalamocortical auditory pathways in primates. In: Burkard, RF.; Don, M.; Eggermont, JJ., editors. Auditory Evoked Potentials: Basic Principles and Clinical Application. Lippincott Williams & Wilkins; Baltimore: 2007b. p. 428-440.

Hackett TA, Stepniewska I, Kaas JH. Subdivisions of auditory cortex and ipsilateral cortical connections of the parabelt auditory cortex in macaque monkeys. J Comp Neurol 1998a;394:475–95. [PubMed: 9590556]

Hackett TA, Stepniewska I, Kaas JH. Thalamocortical connections of the parabelt auditory cortex in macaque monkeys. J Comp Neurol 1998b;400:271–86. [PubMed: 9766404]

Hackett TA, Preuss TM, Kaas JH. Architectonic identification of the core region in auditory cortex of macaques, chimpanzees, and humans. J Comp Neurol 2001;441:197–222. [PubMed: 11745645]

Hackett TA, De La Mothe LA, Ulbert I, Karmos G, Smiley J, Schroeder CE. Multisensory convergence in auditory cortex, II. Thalamocortical connections of the caudal superior temporal plane. J Comp Neurol 2007;502:924–52. [PubMed: 17444488]

Hashikawa T, Rausell E, Molinari M, Jones EG. Parvalbumin-and calbindin-containing neurons in the monkey medial geniculate complex: differential distribution and cortical layer specific projections. Brain Res 1991;544:335–41. [PubMed: 2039948]

Hashikawa T, Molinari M, Rausell E, Jones EG. Patchy and laminar terminations of medial geniculate axons in monkey auditory cortex. J Comp Neurol 1995;362:195–208. [PubMed: 8576433]

Hur EE, Zaborszky L. Vglut2 afferents to the medial prefrontal and primary somatosensory cortices: a combined retrograde tracing in situ hybridization study [corrected]. J Comp Neurol 2005;483:351–73. [PubMed: 15682395]

Jones EG. Chemically defined parallel pathways in the monkey auditory system. Ann N Y Acad Sci 2003;999:218–33. [PubMed: 14681146]

Jones, EG. The Thalamus. Vol. 2. Cambridge University Press; Cambridge: 2007.

Jones EG, Burton H. Areal differences in the laminar distribution of thalamic afferents in cortical fields of the insular, parietal and temporal regions of primates. J Comp Neurol 1976;168:197–247. [PubMed: 821974]

Jones EG, Dell'Anna ME, Molinari M, Rausell E, Hashikawa T. Subdivisions of macaque monkey auditory cortex revealed by calcium-binding protein immunoreactivity. J Comp Neurol 1995;362:153–70. [PubMed: 8576431]

Kaas JH, Hackett TA. Subdivisions of auditory cortex and levels of processing in primates. Audiol Neurootol 1998;3:73–85. [PubMed: 9575378]

Kaas JH, Hackett TA. Subdivisions of auditory cortex and processing streams in primates. Proc Natl Acad Sci U S A 2000;97:11793–9. [PubMed: 11050211]

Kajikawa Y, de la Mothe LA, Blumell S, Hackett TA. A comparison of neuron response properties in areas A1 and CM of the marmoset monkey auditory cortex: tones and broad band noise. J Neurophysiol 2005;93:22–34. [PubMed: 15342713]

Kaneko T, Fujiyama F. Complementary distribution of vesicular glutamate transporters in the central nervous system. Neurosci Res 2002a;42:243–50. [PubMed: 11985876]

Kaneko T, Fujiyama F, Hioki H. Immunohistochemical localization of candidates for vesicular glutamate transporters in the rat brain. J Comp Neurol 2002b;444:39–62. [PubMed: 11835181]

Kharazia VN, Weinberg RJ. Glutamate in thalamic fibers terminating in layer IV of primary sensory cortex. J Neurosci 1994;14:6021–32. [PubMed: 7931559]

Lakatos P, Pincze Z, Fu KG, Javitt DC, Karmos G, Schroeder CE. Timing of pure tone and noise-evoked responses in macaque auditory cortex. Neuroreport 2005;16:933–937. [PubMed: 15931064]

LeDoux JE, Farb CR. Neurons of the acoustic thalamus that project to the amygdala contain glutamate. Neurosci Lett 1991;134:145–9. [PubMed: 1687697]

McMullen NT, de Venecia RK. Thalamocortical patches in auditory neocortex. Brain Res 1993;620:317–22. [PubMed: 7690303]

Mesulam MM, Pandya DN. The projections of the medial geniculate complex within the Sylvian fissure of the rhesus monkey. Brain Res 1973;60:315–333. [PubMed: 4202852]

Molinari M, Dell'Anna ME, Rausell E, Leggio MG, Hashikawa T, Jones EG. Auditory thalamocortical pathways defined in monkeys by calcium-binding protein immunoreactivity. J Comp Neurol 1995;362:171–94. [PubMed: 8576432]

Morel A, Kaas JH. Subdivisions and connections of auditory cortex in owl monkeys. J Comp Neurol 1992;318:27–63. [PubMed: 1583155]

Morel A, Garraghty PE, Kaas JH. Tonotopic organization, architectonic fields, and connections of auditory cortex in macaque monkeys. J Comp Neurol 1993;335:437–59. [PubMed: 7693772]

Nahmani M, Erisir A. VGluT2 immunochemistry identifies thalamocortical terminals in layer 4 of adult and developing visual cortex. J Comp Neurol 2005;484:458–73. [PubMed: 15770654]

O'Kusky J, Colonnier M. A laminar analysis of the number of neurons, glia, and synapses in the adult cortex (area 17) of adult macaque monkeys. J Comp Neurol 1982;210:278–90. [PubMed: 7142443]

Popowits JM, Larue DT, Winer JA. Glutamate is a major transmitter in the rat medial geniculate body. Proc Soc Neurosci 1988;14:490.

Rasmusson DD. The role of acetylcholine in cortical synaptic plasticity. Behavioural Brain Research 2000;115:205–218. [PubMed: 11000421]

Rauschecker JP, Tian B, Hauser M. Processing of complex sounds in the macaque nonprimary auditory cortex. Science 1995;268:111–4. [PubMed: 7701330]

Recanzone GH, Guard DC, Phan ML. Frequency and intensity response properties of single neurons in the auditory cortex of the behaving macaque monkey. J Neurophysiol 2000;83:2315–31. [PubMed: 10758136]

Rudy B, McBain CJ. Kv3 channels: voltage-gated K+ channels designed for high-frequency repetitive firing. Trends Neurosci 2001;24:517–26. [PubMed: 11506885]

Shinonaga Y, Takada M, Mizuno N. Direct projections from the non-laminated divisions of the medial geniculate nucleus to the temporal polar cortex and amygdala in the cat. J Comp Neurol 1994;340:405–26. [PubMed: 8188859]

Varoqui H, Schafer MK, Zhu H, Weihe E, Erickson JD. Identification of the differentiation-associated Na+/PI transporter as a novel vesicular glutamate transporter expressed in a distinct set of glutamatergic synapses. J Neurosci 2002;22:142–55. [PubMed: 11756497]

Velenovsky DS, Cetas JS, Price RO, Sinex DG, McMullen NT. Functional subregions in primary auditory cortex defined by thalamocortical terminal arbors: an electrophysiological and anterograde labeling study. J Neurosci 2003;23:308–316. [PubMed: 12514229]

Weinberger NM. Dynamic regulation of receptive fields and maps in the adult sensory cortex. Annu Rev Neurosci 1995;18:129–58. [PubMed: 7605058]

Wong-Riley M. Changes in the visual system of monocularly sutured or enucleated cats demonstrable with cytochrome oxidase histochemistry. Brain Res 1979;171:11–28. [PubMed: 223730]

Wong TP, Campbell PM, Ribeiro-da-Silva A, Cuello AC. Synaptic numbers across cortical laminae and cognitive performance of the rat during ageing. Neuroscience 1998;84:403–12. [PubMed: 9539212]

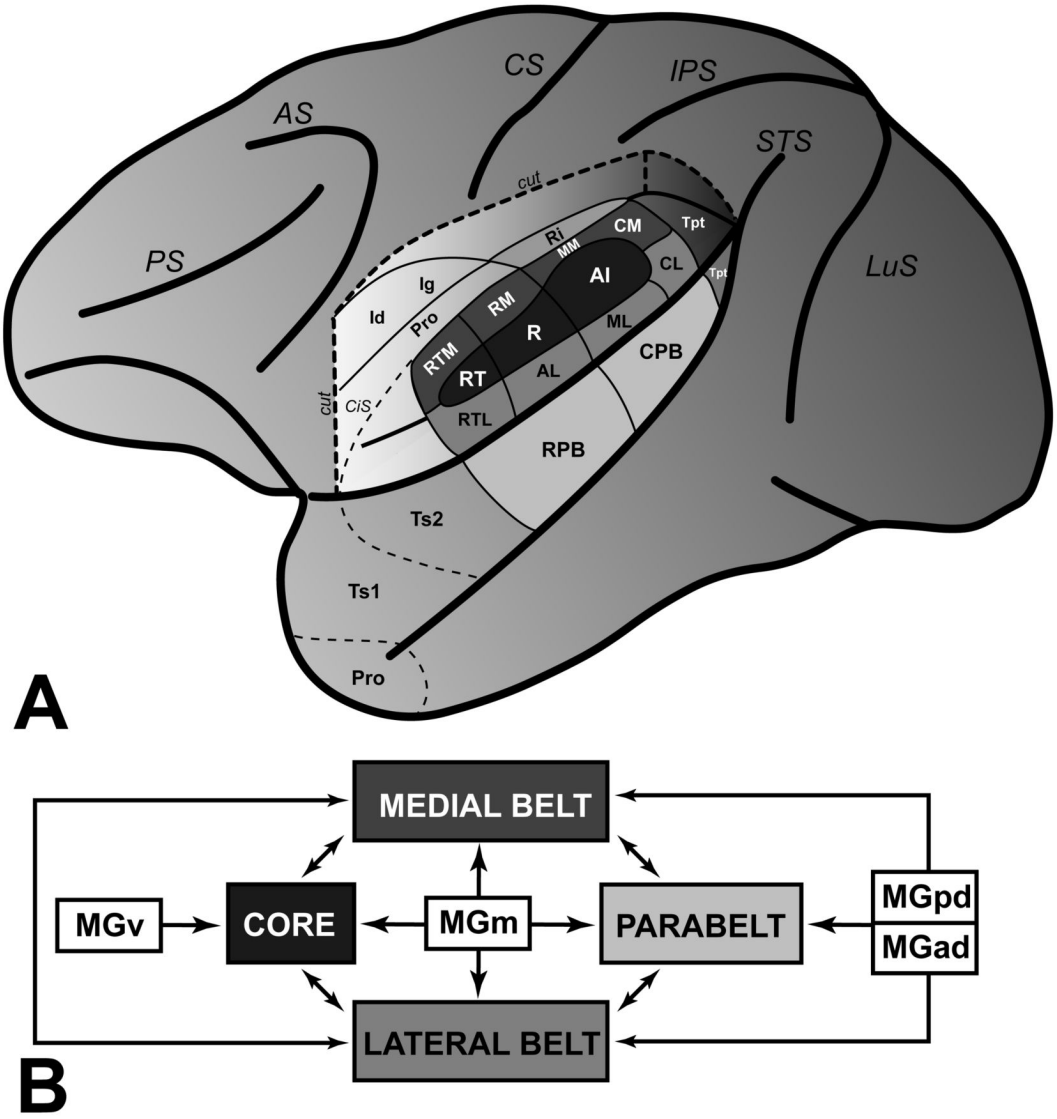

Fig. 1.

Schematic diagrams of auditory cortex organization in the macaque monkey. (A) Left hemisphere with a portion of the parietal cortex removed graphically to show the location of auditory and auditory-related areas on the lower bank of the lateral sulcus (LS). Areas in the core region (A1, R, RT); medial belt region (MM, CM, RM, RTM); lateral belt region (CL, ML, AL, RTL); parabelt region (CPB, RPB). (B) Major patterns of thalamocortical and corticocortical connections between the four major divisions of the medial geniculate complex (MGv, MGad, MGpd, MGm) and regions of auditory cortex, color-coded as in panel A. See list of abbreviations for definitions, and text for other details about these connection patterns.

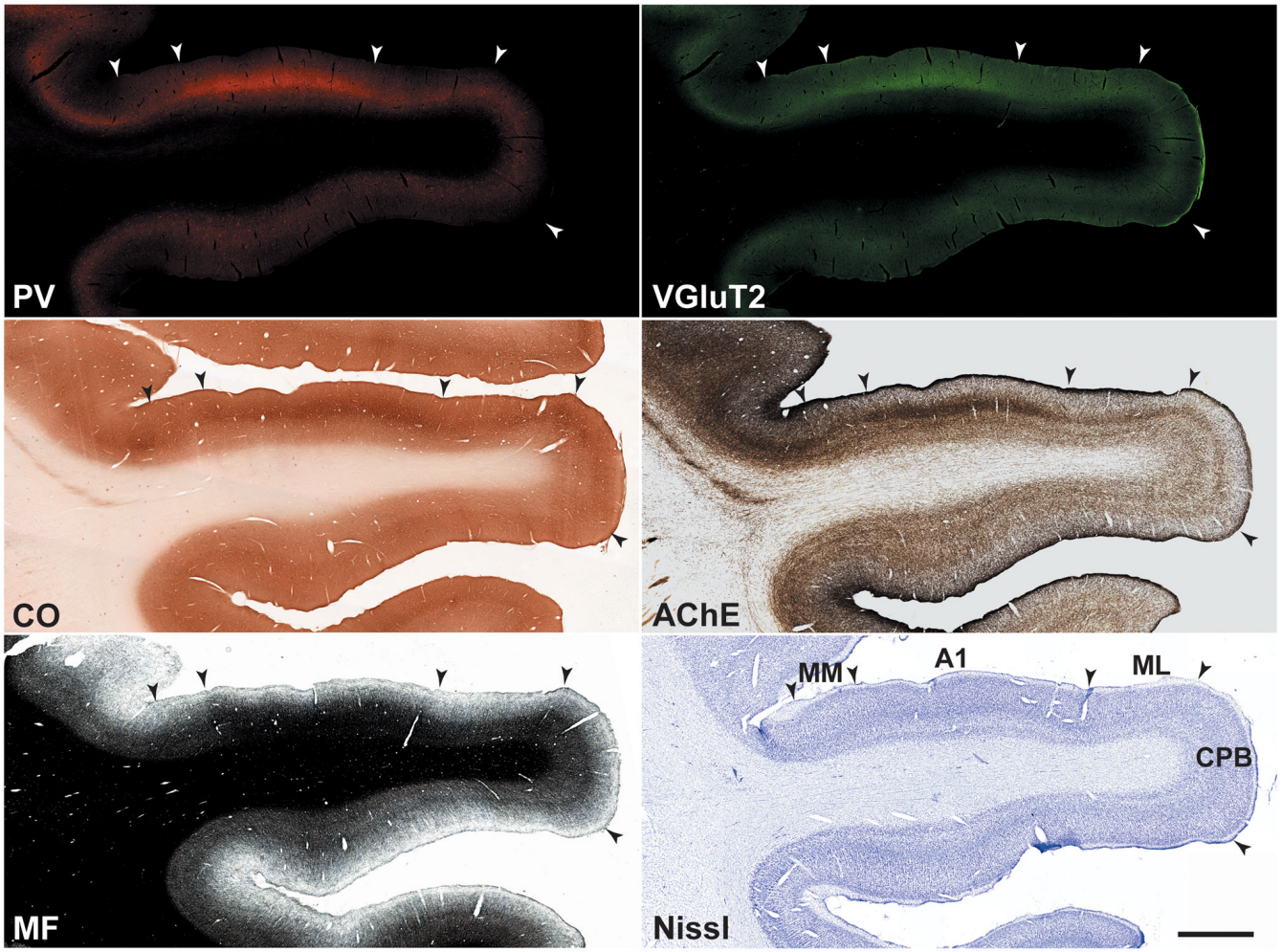

Fig. 2.

Series of adjacent coronal sections through caudal areas of auditory cortex stained for several chemoarchitectonic markers: Parvalbumin (PV), vesicular glutamate transporter 2 (VGluT2); cytochrome oxidase (CO); acetylcholinesterase (AChE); myelinated fibers (MF); Nissl (N). Note that the dense band of staining in layer IIIb/IV is highest in the core area, A1, and weaker in the belt and parabelt areas. Scale bars, 2 mm.

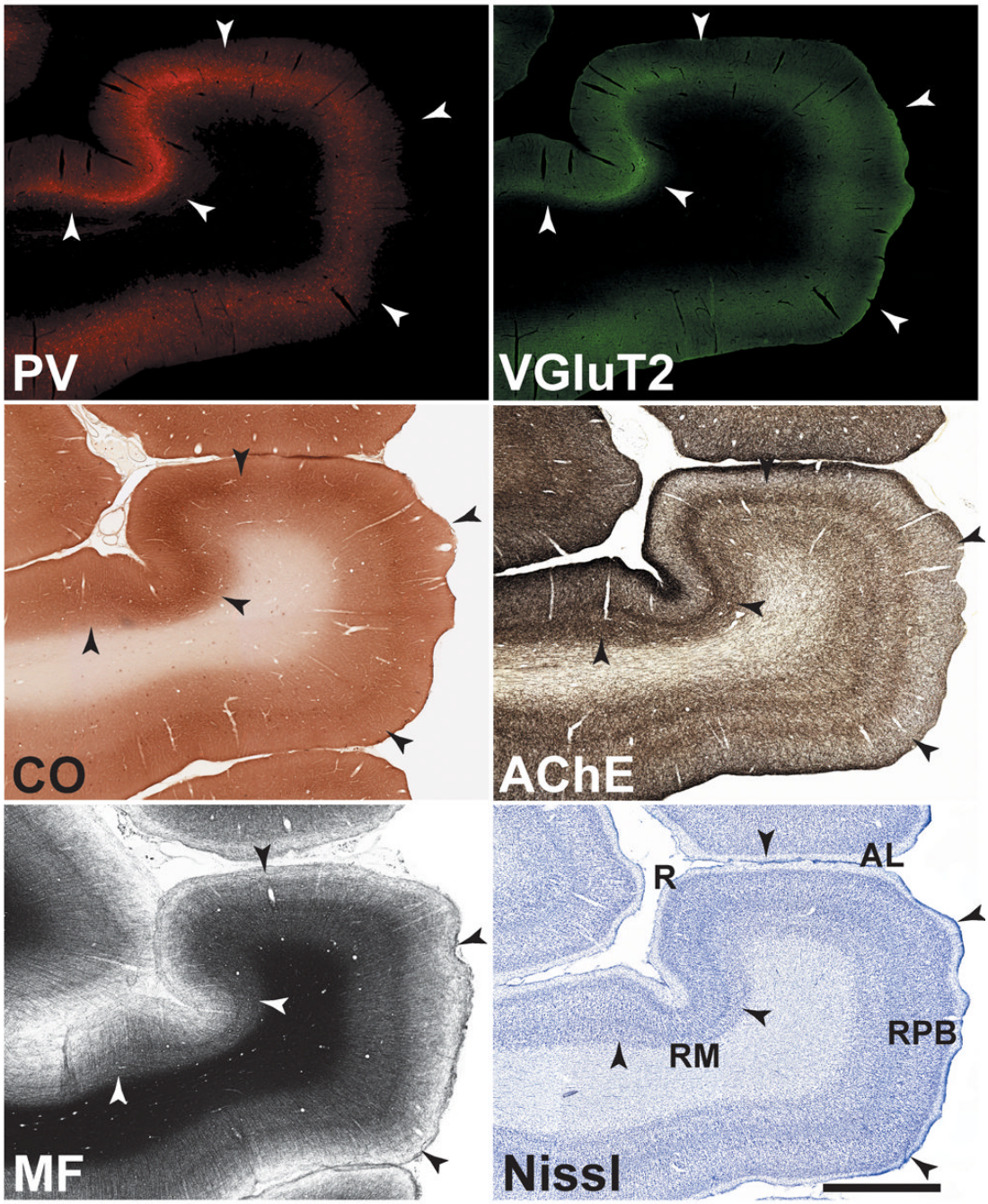

Fig. 3.
Series of adjacent coronal sections through rostral areas of auditory cortex stained for the same chemoarchitectonic markers as Fig. 2. The dense band of staining in layer IIIb/IV is highest in the core area, R, and weaker in the belt and parabelt areas. Scale bars, 2 mm.

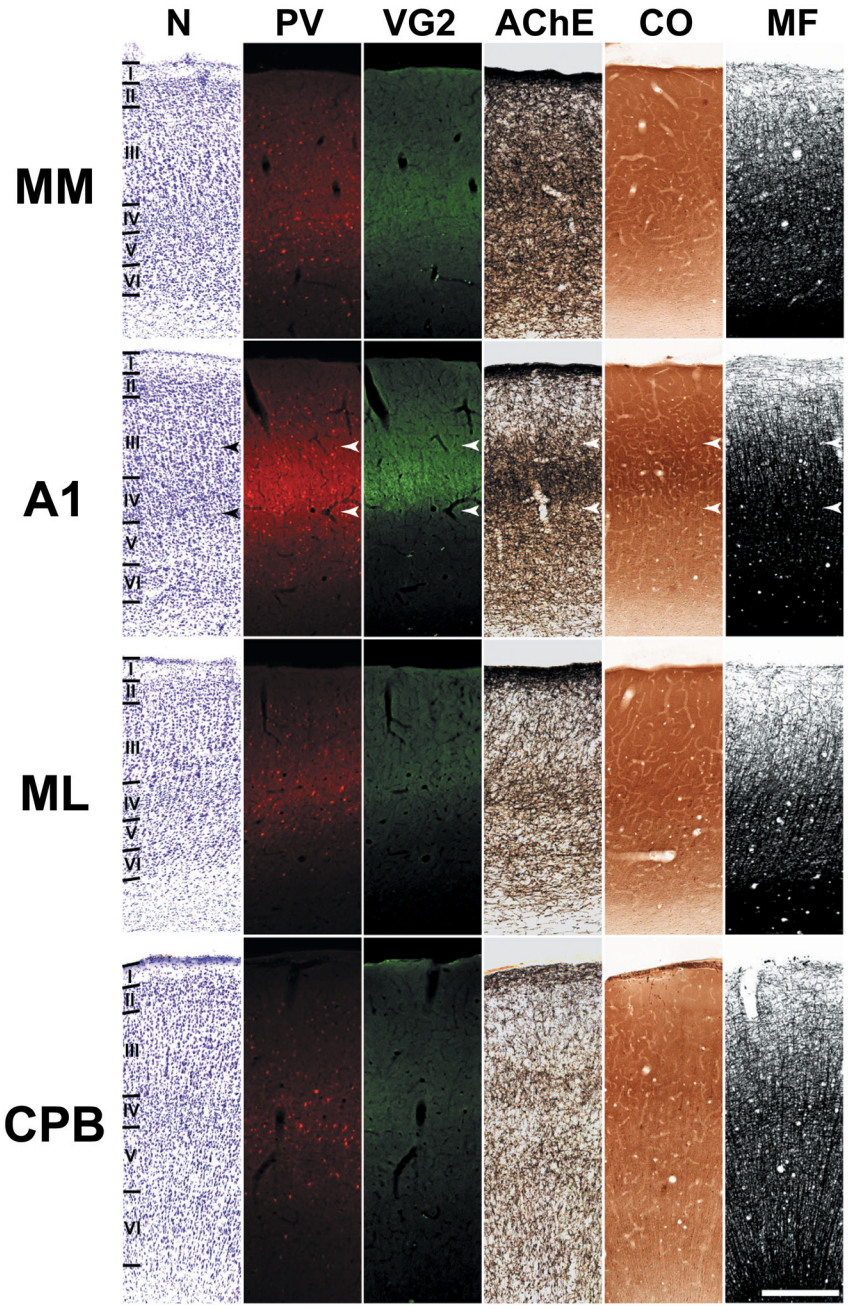

Fig. 4.

Laminar chemoarchitecture in adjoining areas of auditory cortex at the level of A1. Illustrated in each row is a series of adjacent coronal sections for one cortical area stained for the same markers as Figs. 2 and 3. Scale bars, 500 μm.

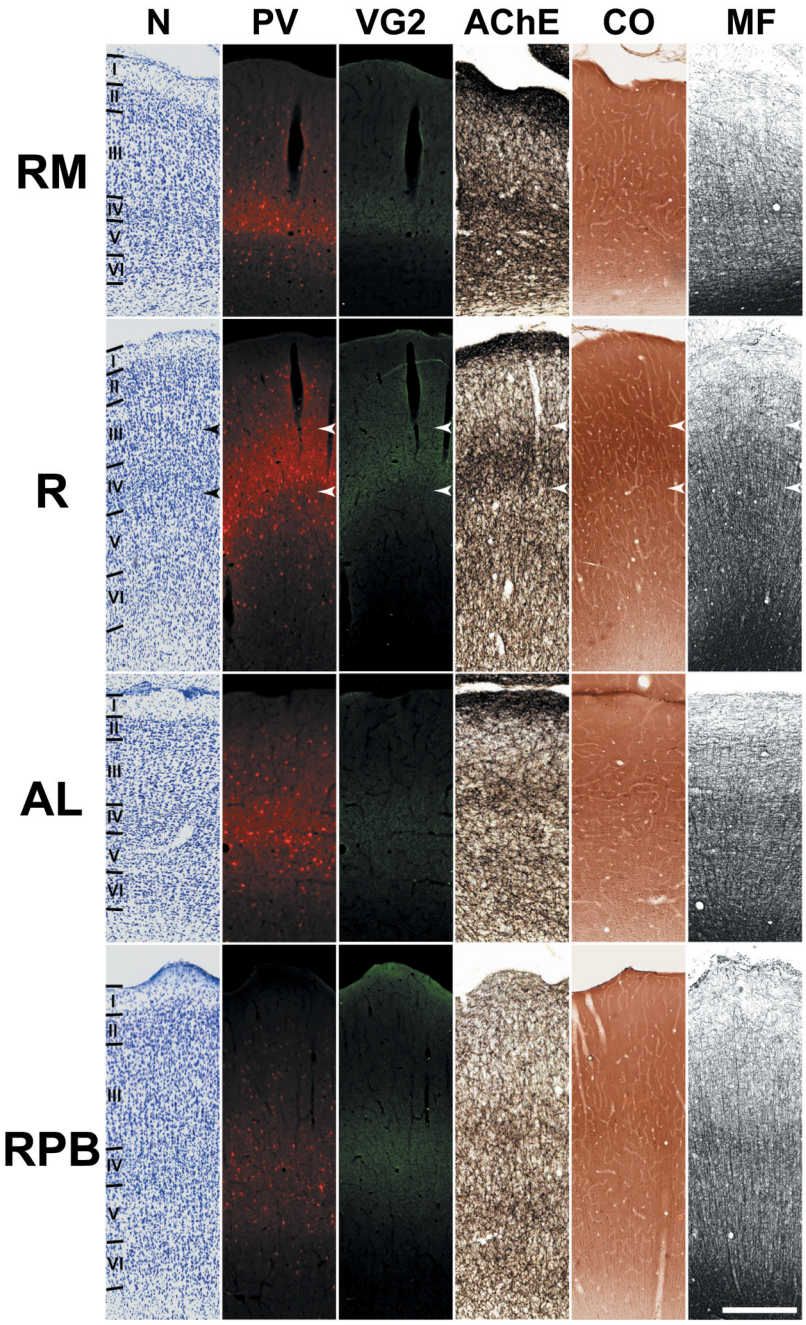

Fig. 5.

Laminar chemoarchitecture in adjoining areas of auditory cortex at the level of R. Illustrated in each row is a series of adjacent coronal sections for one cortical area stained for the same markers as Figs. 2 and 3. Scale bars, 500 μm.

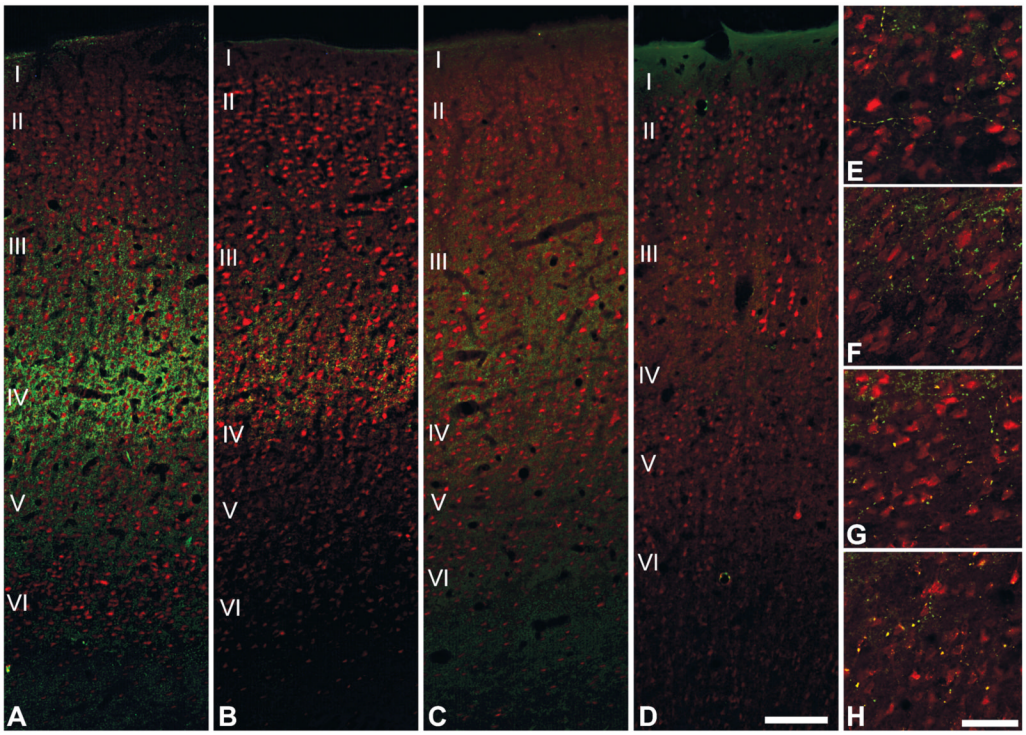

Fig. 6.

Dual fluorescence immunoreactivity for VGluT2 and NeuN in areas A1, MM, ML and CPB. In A1 (A), VGluT2-ir is most densely concentrated in the layers IIIb and IV, where it forms vertical bands around NeuN-ir cell columns. In MM (B), VGluT2-ir is most dense in IIIb with some extension into layer IV. In ML (C), VGluT2-ir is reduced compared to MM and mainly concentrated in IIIb. VGluT2-ir is absent in the IIIb/IV band of the CPB (D). (E – H) In all areas, sparse VGluT2-ir is contained in boutons en passant positioned along local axon branches in layers Vb and VI. Scale bars: 250 μm (A–D), 25 μm (E–H).

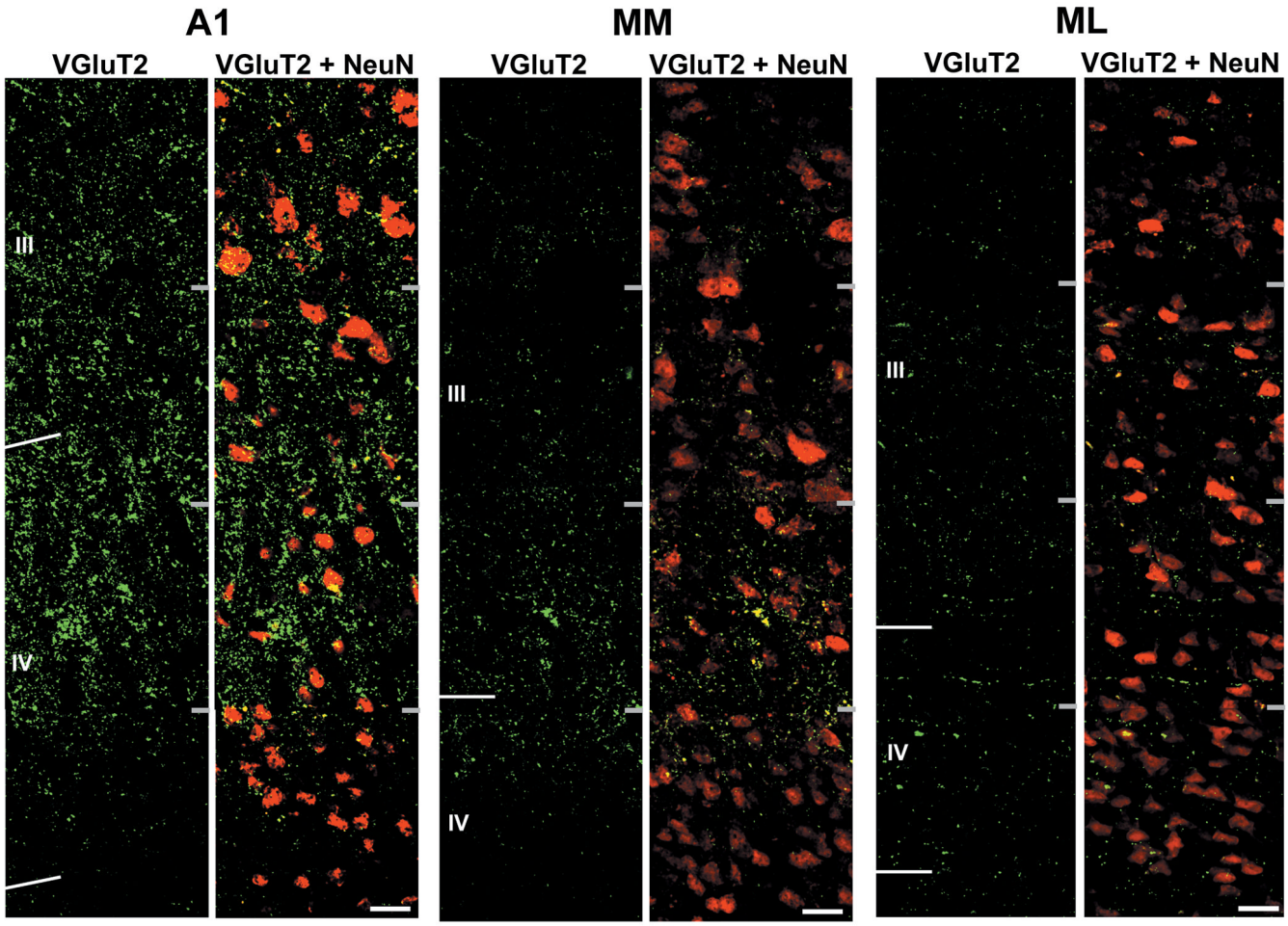

Fig. 7.

Dual fluorescence confocal images of VGluT2-r and NeuN-r in areas A1, MM, and ML. Each image is a 4-panel confocal montage collapsed over the z-axis spanning layers III and IV. Tick marks at the right side of each image denote the bottom of each panel in the montage. Laminar boundaries are indicated by angled tick marks on the left side of each image. Scale bar, 20 μm.

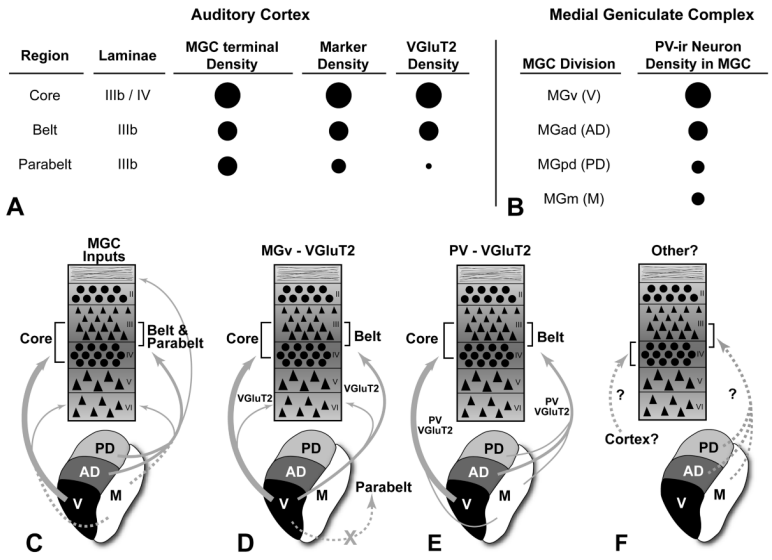

Fig. 8.

Summary and interpretations of results. (A) Tabular representation showing relative densities of MGC axon terminals, chemoarchitectonic markers (CO, AChE, PV), and VGluT2 in layers IIIb and IV of the core, belt, and parabelt. Larger circles denote highest density; (B) Tabular representation of relative PV-ir neuron density in each division of the MGC; (C) Laminar projections (arrows) to auditory cortical regions from major divisions of the MGC. Line thickness denotes relative density of each projection. Dashed line for MGm indicates that the proportion of total inputs from neurons in this division is unknown. (D) Interpretation 1: VGluT2 density differences between regions of auditory cortex reflects MGv inputs. Note, MGv does not project to the parabelt ("X"). (E) Interpretation 2: VGluT2 density reflects density of PV-ir neurons in each MGC division. (F) Some inputs to the layer IIIb/IV band from cortex or thalamus may utilize a different VGluT or neurotransmitter. MGC divisions: V, ventral; AD, anterodorsal; PD, posterodorsal; M, magnocellular. See text for details.

TABLE 1

Details of primary and secondary antibodies used. For each antibody, species (type), concentration in incubation solution (Dilution), commercial source and catalogue number (Source, Cat #), and information about antigen specificity are given.

Primary and secondary antibodies used.

Primary Antibody	Type	Dilution	Source	Cat #	Antigen specificity
VGluT2	Monoclonal	1:1000	Chemicon	MAB5504	Rat hypothalamus (Hrabovszky et al., 2006); rat cortex (Fremeau et al., 2001)
PV	Monoclonal	1:2000	Sigma	P3088	Rat cortex (Celio, 1990; Kawaguchi and Kubota, 1997).
NeuN	Monoclonal	1:1000	Chemicon	MAB377	Mouse cortex, cerebellum (Lind et al., 2005; Mullen et al., 1992).
Secondary Antibody	**Type**	**Dilution**	**Source**	**Cat #**	**Color**
Alexa-fluor 405 IgG	Goat anti-mouse	1:200	Invitrogen	A31553	Blue
Alexa-fluor 488 IgG	Goat anti-mouse	1:200	Sigma	A11001	Green
Alexa-fluor 594 IgG	Goat anti-mouse	1:200	Chemicon	A11005	Red